electronic materials

MDPI

Brief Report

An Investigation of Proton Conductivity in Zeolite Beta Composite Membranes: Towards Quasi-Solid-State Proton Batteries

Christopher O'Loughlin [1], Eric Jones [1], Alcina DaCosta [1], Grant Strohmeyer [1] and Theda Daniels-Race [1,2,*]

[1] Division of Electrical and Computer Engineering, Louisiana State University, 3325 Patrick F. Taylor Hall, Baton Rouge, LA 70803, USA; coloughlin@lsu.edu (C.O.); ejone97@lsu.edu (E.J.); tcosta5@lsu.edu (A.D.); grant.strohmeyer@lsu.edu (G.S.)
[2] Center for Computation & Technology, Louisiana State University, 888 S. Stadium Dr., Baton Rouge, LA 70808, USA
* Correspondence: tdrace@lsu.edu

Abstract

Zeolite composite membranes provide a compelling path toward stable quasi-solid proton electrolytes. This study evaluates the through-plane proton conductivity of H-form Zeolite Beta/polyvinylidene fluoride (H-Beta:PVDF) membranes post-activation in aqueous sulfuric acid. Membranes were characterized via electrochemical impedance spectroscopy between blocking electrodes and modeled using an $R_s + (R_b \| \mathrm{CPE}_b)$ equivalent circuit where R_s is the series resistance, R_b is the bulk resistance, and CPE_b is the bulk constant phase element. Apparent ionic conductivities ranged from 2.31×10^{-6} to 1.53×10^{-5} S cm^{-1}. Bulk CPE exponents were observed between 0.42 and 0.87, suggesting non-ideal impedance responses.

Keywords: zeolite; BEA; H-Beta zeolite; composite membranes; quasi-solid electrolytes; proton conductivity; electrochemical impedance spectroscopy; proton batteries

1. Introduction

Batteries have become a cornerstone in the sustainable energy economy, with global demand projected to rise [1]. Lithium-ion technologies currently dominate across applications; however, associated concerns in regard to costs and sustainability highlight the need for post-lithium technologies [1,2]. Due to their unique characteristics, proton batteries (PBs) are gaining research attention as a post-lithium energy storage platform.

Utilizing protons (H^+) as charge carriers, PBs can exhibit rapid charge/discharge behavior due to the unique transport properties of hydrogen ions [3]. In hydrated environments within an applied potential, proton conduction can occur through the Grotthuss mechanism, in which H^+ transfers through hydrogen-bonded water networks via successive proton-transfer events supporting high proton conductivity [3]. When absorbed within porous solid matrices, these species may form connected hydrated pathways that enable proton conduction [4–6].

This study investigates the proton conductivity of H-form Zeolite Beta/binder composite membranes after activation with aqueous sulfuric acid. A key challenge for zeolitic quasi-solid electrolytes is to maintain continuous pathways for hydrated proton transport while minimizing binder-driven obstructions [3–5,7]. The framework of H-Form zeolite Beta (H-Beta) is advantageous for this objective due to its three-dimensional, large, approximately 6.7 Å pore network with an accessible volume in the range of 19–21% [8,9].

Check for updates

Academic Editor: Hirofumi Yoshikawa

Received: 9 September 2026
Revised: 19 October 2026
Accepted: 26 October 2026
Published: 30 October 2026

Copyright: © 2026 by the authors. Licensee MDPI, Basel, Switzerland. This article is an open access article distributed under the terms and conditions of the Creative Commons Attribution (CC BY) license.

These features may support aqueous acid uptake and hydrated proton availability, which may increase the likelihood of the formation of percolating proton conduction pathways. Optimizing H-Beta to binder ratios may help limit pathway constrictions.

2. Materials and Methods

H-form Zeolite Beta (H-Beta) with a Si:Al ratio of 180 was the material studied. Although H-form provides Brønsted acid sites, the high Si:Al ratio suggests that intrinsic framework acidity is limited [6]; therefore, conductivity is more plausibly associated with retained hydrated sulfuric-acid domains within the H-Beta composite. Polyvinylidene fluoride (PVDF) was selected as a mechanically stable polymer binder with which to support and integrate the bulk zeolite matrix. N-methyl-2-pyrrolidone (NMP) was selected as a suitable casting solvent with which to dissolve PVDF, forming a homogeneous PVDF/NMP slurry suitable for membrane casting [10,11].

Aqueous H_2SO_4 was selected as a proton source due to sulfuric acid's wide use in electrochemical studies that require high proton availability [12,13]. Concentrations of 0.5 and 1.0 M were used to support proton transport while avoiding unnecessarily corrosive conditions. Gold electrodes were used to block faradaic charge-transfer reactions, isolating ionic transport through the saturated H-Beta/PVDF membranes during Electrochemical Impedance Spectroscopy (EIS). Gold provides ideal characteristics such as high electrical conductivity, chemical stability, resistance to passivating oxide formation, and blocking toward proton transfer [14–16].

PVDF was dissolved in NMP and stirred for 2 h. Zeolite powders were dried at 120 °C for 12 h, added to the PVDF/NMP solution, and stirred for 30–60 min to prepare the casting slurries. The slurries were then cast onto gold-plated electrode foil and degassed overnight at 50 °C. The resultant electrode-supported H-Beta/PVDF films were diced into 16 mm diameter discs and soaked in sulfuric acid for 4 h for activation. After activation, the cast was stacked with an opposing Au-plated blocking electrode and assembled into a standard 2032-coin cell. EIS spectroscopy measurements were performed immediately after assembly. Table 1 lists the composition, preparation conditions, and dimensions of the 11 H-Beta/PVDF specimens discussed in this work. The data used in this study are provided in the Supplementary Materials.

Table 1. Summary of sample composition, preparation and dimensions regarding the 11 H-Beta/PVDF specimens discussed in this work.

Sample	H-Beta Mass Fraction	H_2SO_4 (M)	NMP (mL)	Thk (µm)	Dia. (mm)
S7	0.8	0.5	2.4	96	15
S10	0.85	0.5	2	186	15
S14	0.85	0.5	2	136	15
S18	0.8	1	2.4	96	15
S22	0.9	1	3	82	15
S24	0.85	1	2.4	142	15
S25	0.85	1	2.4	115	14
S26	0.8	1	2	224	14
S27	0.8	1	2	224	14
S29	0.8	1	2	224	14
S30	0.8	1	2	224	15

Potentiostatic EIS was performed using Admiral Instruments Squidstat Plus to evaluate the through-plane ionic conductivity of H-Beta composite membranes. Membranes were configured between two Au-plated blocking electrodes and measured over a range of 10 MHz–10 mHz with a 10 mV perturbation. The dominant arc of the measured Nyquist spectra was fitted to the equivalent circuit $R_s + (R_b \| \mathrm{CPE}_b)$ using the standard CPE impedance [17],

$$Z_{\mathrm{CPE}_b}(\omega) = \frac{1}{Q_b(j\omega)^{n_b}}, \quad (1)$$

with the corresponding impedance function obtained by combining the parallel branch admittances and adding the series resistance:

$$Z(\omega) = R_s + \left[\frac{1}{R_b} + Q_b(j\omega)^{n_b}\right]^{-1}. \quad (2)$$

where R_s is the series resistance, R_b is bulk membrane resistance, CPE_b is the constant phase element associated with the bulk membrane response, $Z(\omega)$ is the total complex impedance at angular frequency ω, Q_b is the CPE coefficient for the bulk membrane response, and n_b is the dimensionless CPE exponent [15,17]. The equivalent-circuit parameters were determined by simultaneous unweighted least-squares fitting of the real and imaginary impedance components.

Further, Raman spectroscopy was used to assess any potential changes in the composite membrane chemistry before and after EIS cycling by comparing characteristic peak positions and spectral profiles.

3. Results

Acid-activated H-Beta/PVDF composite membranes exhibited measurable through-plane apparent ionic conductivity after acid activation, with the sample set giving a conductivity in the range of $2.31 \times 10^{-6} \leq \sigma_b \leq 1.53 \times 10^{-5}$ S cm^{-1} and a median of $\sigma_{\mathrm{median}} = 9.79 \times 10^{-6}$ S/cm. In contrast, dry membranes exhibited an open-circuit response, while membranes hydrated with water alone exhibited conductivities greater than 4.90×10^{-8} S/cm. These values indicate that acid activation of H-Beta/PVDF membrane composites greatly increases their proton conduction relative to water-alone hydration. The fitted bulk resistance ranged from 587 to 2860 Ω, with a median of 1040 Ω. The corresponding median area-specific resistance was $\mathrm{ASR}_{\mathrm{median}} = 1.90$ kΩ cm^2. The fitted CPE exponent range was $0.42 \leq n \leq 0.87$, consistent with depressed Nyquist arcs and a non-ideal impedance response through heterogeneous composite membranes [17,18]. This non-ideal behavior may reflect variations in particle dispersion, hydration, binder-induced pathway constrictions, and electrode–membrane contact [7,18], indicating that further refinement of the mix and casting process may improve homogeneity and percolating proton pathways. Figure 1a presents a representative Nyquist plot with a fitted model curve and an observable low-frequency tail. Figure 1b is an overlay of the raw Nyquist data discussed in this work.

Untreated and post-cycling H-Beta membranes exhibited similar Raman profiles over 300–1000 cm^{-1}, and representative Raman spectra are presented in Figure 2. Comparison of the spectra was focused on the 300–700 cm^{-1} framework-sensitive region (highlighted in Figure 2), where zeolite rings and T–O–T vibrational modes are commonly observed [19]. Here, T denotes a tetrahedrally coordinated Si or Al atom, and O denotes the bridging oxygen atom. The preservation of the overall spectral pattern suggests that there was no major Raman-detectable difference in the H-Beta framework following acid activation and EIS cycling.

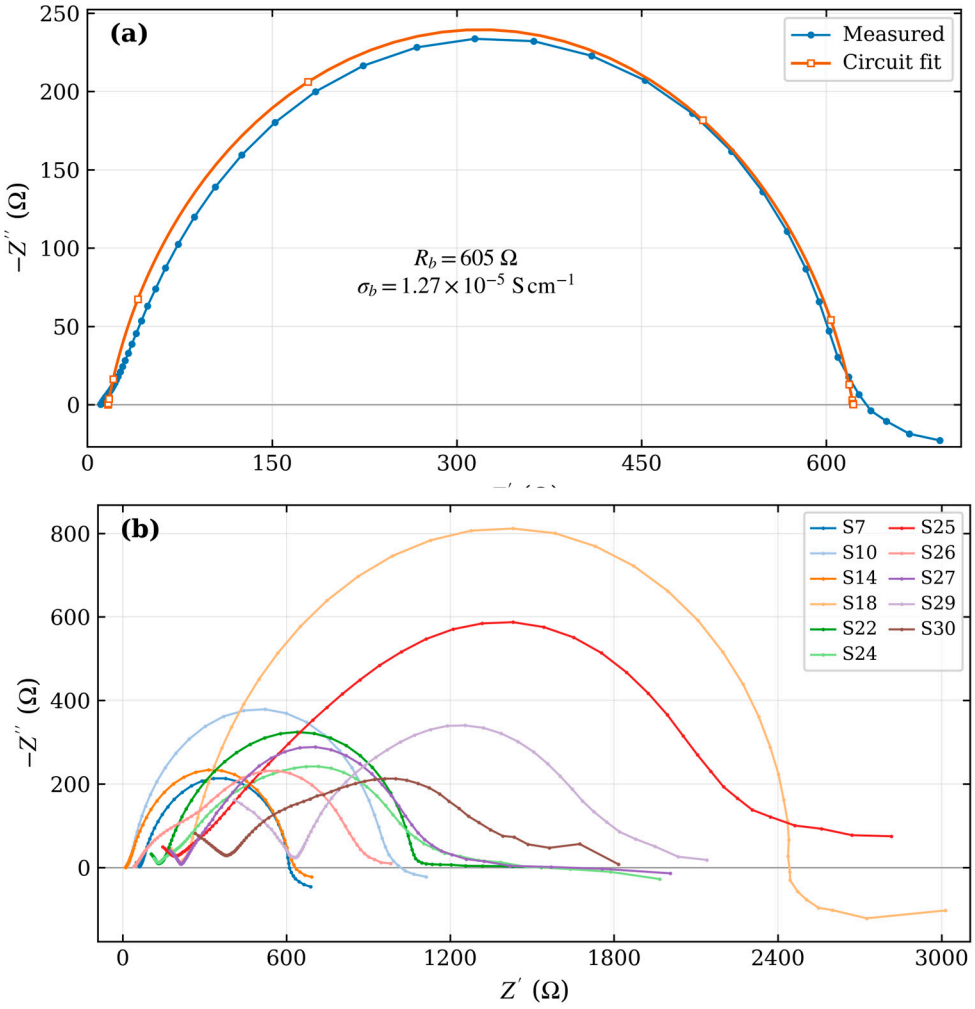


Figure 1. Electrochemical impedance characterization of H-Beta composite membranes. (**a**) A representative Nyquist Plot from a single sample source with the measured response and equivalent-circuit model fit. (**b**) Nyquist response overlay of sample set.

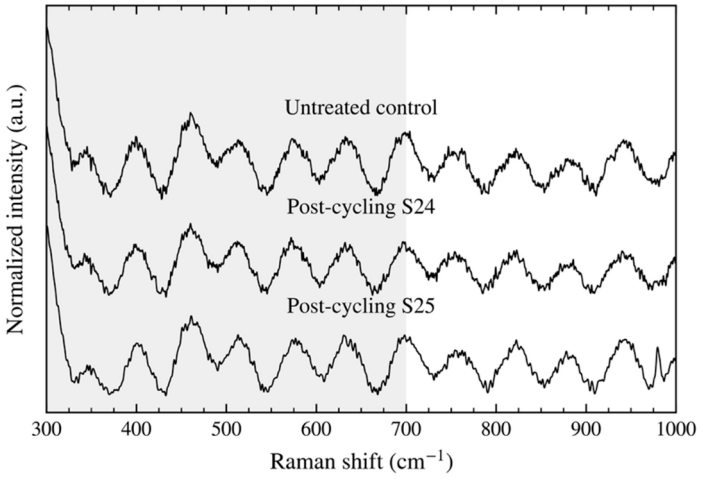


Figure 2. Raman shift of untreated zeolite composite compared to two post-cycled membranes with region of interest highlighted in grey.

4. Discussion

The 0.5 M group exhibits a higher average σ_b than the 1.0 M group in the present dataset; however, this trend cannot be established as an independent effect of acid concentration without further controlled study, as the samples also differ in thickness, composition, and slurry volumes. Likewise, an independent effect of the H-Beta:PVDF ratio cannot be determined. Membrane morphology, hydration, and the electrode interface may contribute to the observed variability, but these contributions remain unresolved. Furthermore, proton selectivity, transport mechanisms, and the relative contribution of retained acid and zeolite-associated pathways remain unresolved. However, the relative increase in ion conductivity observed in acid-activated membranes calls for further controlled studies varying one parameter at a time to distinguish these effects.

The median ASR of 1.90 kΩ cm^2 can correspond to a large ohmic voltage drop. At an illustrative current density of 1 mA cm^{-2}, the implied ohmic voltage drop is 1.9 V, representing a substantial limitation to practical battery operation. Due to this limitation, reducing membrane thickness and increasing ionic conductivity while targeting improved aqueous acid uptake are priorities in developing such materials for battery applications.

It is also notable that both the high-silica H-Beta and PVDF binder used exhibit relatively hydrophobic characteristics. Consequently, reducing the Si/Al ratio of H-Beta and incorporating a more hydrophilic binder may improve aqueous uptake, thus promoting the formation of ionic pathways.

5. Conclusions

In conclusion, aqueous sulfuric acid activation of H-Beta/PVDF composite membranes was demonstrated to substantially improve apparent through-plane conductivity. However, the fitted bulk CPE exponents, ranging from 0.42 to 0.87, indicate a non-ideal impedance response but do not establish a specific transport mechanism. Further refinement of membrane fabrication and materials may improve aqueous acid uptake, homogeneity, and the connectivity of ion pathways. These findings provide motivation for further investigation into proton-selective transport and the underlying conduction mechanisms through complementary proton-permeation and membrane-potential measurements.

Supplementary Materials: The following supporting information can be downloaded at: https://www.mdpi.com/article/10.3390/electronicmat7040029/s1.

Author Contributions: The authors have contributed to this work as follows: Conceptualization, C.O. and T.D.-R.; methodology, C.O. and T.D.-R.; software, E.J.; validation, C.O., A.D., G.S. and T.D.-R.; formal analysis, C.O. and E.J.; investigation, C.O., A.D. and G.S.; resources, T.D.-R.; data curation, C.O., E.J. and T.D.-R.; writing, C.O.; writing—review and editing, T.D.-R.; visualization, C.O.; supervision, T.D.-R.; project administration, T.D.-R.; funding acquisition, T.D.-R. All authors have read and agreed to the published version of the manuscript.

Funding: This research was partially funded by the generous support provided by Dr. Kristina Johnson via Louisiana State University (LSU) Foundation ID project #104454. This work was also partially supported by funds from the corresponding author's Michel B. Voorhies Distinguished Professorship, LSU Foundation project #101541.

Data Availability Statement: The original contributions presented in this study are included in the article/Supplementary Materials. Further inquiries can be directed to the corresponding author.

Acknowledgments: During the preparation of this manuscript, the authors used OpenAI's ChatGPT (OpenAI; used May–October 2026) and Grammarly (used May–October 2026) to assist with improving the linguistic clarity of the manuscript. ChatGPT was also used to develop Python 3.12 code using NumPy 2.3.5, SciPy 1.17, pandas 2.2.3, Matplotlib 3.10.8 code for the least-squares fitting of author-generated experimental Nyquist data to the equivalent-circuit model and plotting of the raw Nyquist

data alongside corresponding fitted model curves. For selected samples, the fitted parameters R_b, Q_b and n_b were checked for consistency with estimates derived from raw EIS data. The authors performed the scientific analysis and interpretation. All data processing, code, numerical results, and figures were reviewed and verified by the authors, who take full responsibility for the content of the published article.

Conflicts of Interest: The authors declare no conflicts of interest.

References

1. IEA. *Batteries and Secure Energy Transitions*; IEA: Paris, France, 2024. Available online: https://www.iea.org/reports/batteries-and-secure-energy-transitions (accessed on 15 May 2026).
2. Graeber, G.; Thatipamula, V.S. Beyond lithium-ion batteries: Shaping the transition to sustainable electrochemical energy storage. *MIT Sci. Policy Rev.* **2022**, *3*, 66–72. [CrossRef]
3. Guo, H.; Zhao, C. An Emerging Chemistry Revives Proton Batteries. *Small Methods* **2024**, *8*, 2300699. [CrossRef]
4. Xu, Z.; Michos, I.; Cao, Z.; Jing, W.; Gu, X.; Hinkle, K.; Murad, S.; Dong, J. Proton-Selective Ion Transport in ZSM-5 Zeolite Membrane. *J. Phys. Chem. C* **2016**, *120*, 26386–26392. [CrossRef]
5. Iskhakova, L.; Cao, Z.; Sun, X.; Gabski, J.; Dong, J. Preactivated zeolite nanosheet plate-tiled membrane on porous PVDF film: Synthesis and study of proton-selective ion conduction. *J. Membr. Sci.* **2023**, *669*, 121328. [CrossRef]
6. Franke, M.E.; Simon, U. Solvate-supported proton transport in zeolites. *Chemphyschem* **2004**, *5*, 465–472. [CrossRef]
7. Zapata, P.; Lee, J.-H.; Meredith, J.C. Composite proton exchange membranes from zirconium-based solid acids and PVDF/acrylic polyelectrolyte blends. *J. Appl. Polym. Sci.* **2012**, *124*, E241–E250. [CrossRef]
8. Database of Zeolite Structures. Available online: https://www.iza-structure.org/databases/ (accessed on 15 May 2026).
9. Zieliński, M.; Matysiak, N.; Janiszewska, E. Rational Design of Hierarchical Beta Zeolites via Post-Synthesis Treatments and Their Applications. *Molecules* **2025**, *30*, 1030. [CrossRef]
10. Abdul Wahab, M.S.; Abd Rahman, S. Production of Mixed Matrix (PVDF/Zeolite) Membrane for CO_2/N_2 Gas Separation. *Int. J. Chem. Biomol. Sci.* **2015**, *1*, 264–270.
11. Ma, Y.; Chang, L.; Yi, D.; Liu, M.; Wang, P.; Luo, S.; Zhang, Z.; Yuan, Y.; Lu, H. Synergetic effect of block and catalysis on polysulfides by functionalized bilayer modification on the separator for lithium-sulfur batteries. *Energy Mater.* **2024**, *4*, 400059. [CrossRef]
12. Yang, X.; Ni, Y.; Lu, Y.; Zhang, Q.; Hou, J.; Yang, G.; Liu, X.; Xie, W.; Yan, Z.; Zhao, Q.; et al. Designing Quinone-Based Anodes with Rapid Kinetics for Rechargeable Proton Batteries. *Angew. Chem. Int. Ed.* **2022**, *61*, e202209642. [CrossRef]
13. Slade, S.; Campbell, S.A.; Ralph, T.R.; Walsh, F.C. Ionic Conductivity of an Extruded Nafion 1100 EW Series of Membranes. *J. Electrochem. Soc.* **2002**, *149*, A1556. [CrossRef]
14. Vilela, S.M.F.; Salcedo-Abraira, P.; Gómez-Peña, A.; Trens, P.; Várez, A.; Salles, F.; Horcajada, P. Proton Conductive Zr-Phosphonate UPG-1—Aminoacid Insertion as Proton Carrier Stabilizer. *Molecules* **2020**, *25*, 3519. [CrossRef]
15. Soboleva, T.; Xie, Z.; Shi, Z.; Tsang, E.; Navessin, T.; Holdcroft, S. Investigation of the through-plane impedance technique for evaluation of anisotropy of proton conducting polymer membranes. *J. Electroanal. Chem.* **2008**, *622*, 145–152. [CrossRef]
16. Chen, P.; Simon, U. In Situ Spectroscopic Studies of Proton Transport in Zeolite Catalysts for NH3-SCR. *Catalysts* **2016**, *6*, 204. [CrossRef]
17. Mikhailenko, S.D.; Guiver, M.D.; Kaliaguine, S. Measurements of PEM conductivity by impedance spectroscopy. *Solid State Ion.* **2008**, *179*, 619–624. [CrossRef]
18. Jorcin, J.-B.; Orazem, M.E.; Pébère, N.; Tribollet, B. CPE analysis by local electrochemical impedance spectroscopy. *Electrochim. Acta* **2006**, *51*, 1473–1479. [CrossRef]
19. Wang, T.; Luo, S.; Tompsett, G.A.; Timko, M.T.; Fan, W.; Auerbach, S.M. Critical Role of Tricyclic Bridges Including Neighboring Rings for Understanding Raman Spectra of Zeolites. *J. Am. Chem. Soc.* **2019**, *141*, 20318–20324. [CrossRef]

Disclaimer/Publisher's Note: The statements, opinions and data contained in all publications are solely those of the individual author(s) and contributor(s) and not of MDPI and/or the editor(s). MDPI and/or the editor(s) disclaim responsibility for any injury to people or property resulting from any ideas, methods, instructions or products referred to in the content.